Supporting Information

Efficient Surface Modulation of Single-Crystalline $Na_2Ti_3O_7$ Nanotube Arrays with Ti^{3+} Self-Doping toward Superior Sodium Storage

Jinlong Liu,[†,‡] Zhenyu Wang,[‡] Zhouguang Lu,[‡] Lei Zhang,[†] Fangxi Xie,[†] Anthony Vasileff,[†] and Shi-Zhang Qiao[,†]*

[†]Center for Materials in Energy and Catalysis, School of Chemical Engineering and Advanced Materials, The University of Adelaide, Adelaide, SA 5005, Australia

[‡]Department of Materials Science and Engineering, Southern University of Science and Technology, Shenzhen 518055, P.R. China

[*]Corresponding Author: Shi-Zhang Qiao, E-mail address: s.qiao@adelaide.edu.au.

1. Experimental Section

1.1 Synthesis of Materials

N-NTO NTAs was synthesized via a combination of hydrothermal reaction and NH_3-assisted calcination. Typically, a piece of Ti foil (2 cm × 4 cm) was cleaned with deionized water, acetone and ethanol subsequently under sonication. To prepare the hydrothermal solution, 1.6 g of sodium hydroxide was dissolved into 40 mL of deionized water by magnetic stirring for 10 min. Afterwards, the solution was transferred into a 50 mL Teflon-lined stainless-steel autoclave, and the cleaned Ti foil was immersed into the solution. The autoclave was then sealed and kept in a preheated oven at 220 °C for 10 h. After cooling down naturally to ambient temperature, NTO NTAs was collected by rinsing with water and ethanol several times and further drying in a vacuum oven at 60 °C overnight. Finally, the precursor NTO NTAs was moved to a combustion boat, which was loaded in a tube furnace and annealed in NH_3/Ar (5:95 by volume) atmosphere at 500 °C for 2 h with a ramp rate of 2 °C min^{-1}. For comparison, A-NTO NTAs was prepared through the same thermal treatment of precursor NTO NTAs except for the pure Ar atmosphere. The mass loading of $Na_2Ti_3O_7$ is about 0.8 mg cm^{-2} for both N-NTO NTAs and A-NTO NTAs, which is calculated by the mass difference between the resultant N-NTO NTAs/A-NTO NTAs and the underlying substrate. Briefly, the mass of as-prepared N-NTO NTAs/A-NTO NTAs (M) can be determined by direct weighting on an analytical balance. Then, the $Na_2Ti_3O_7$ nanoarrays can be removed via scraping using a scalpel to give the underlying substrate, whereby the mass of Ti substrate (m) can also be read on the analytical balance. In this way, the mass loading can be evaluated as (M – m)/2×A, where A is the geometric area of N-NTO NTAs/A-NTO NTAs.

1.2 Material Characterizations

Characterizations were carried out employing field emission scanning electron microscope (SEM, FEI Quanta 450 FEG), scanning transmission electron microscope (S/TEM, Tecnai G^2 F30) with high-angle annular dark-field (HADDF) detector and X-ray energy dispersive spectroscopy (EDS), X-ray powder diffraction (XRD, Rigaku MiniFlex 600 X-ray diffractometer, Cu Kα radiation), Raman (iHR550 spectrometer, 532-nm laser wavelength) and X-ray photoelectron spectroscopy (XPS, ESCALab250 XPS spectrometer).

1.3 Electrochemical Measurements

Electrochemical measurements were conducted by assembling 2032 type coin cells in an Ar-filled glovebox (MBRAUN). To be specific, as-obtained N-NTO NTAs and A-NTO NTAs

were scraped off from one side of Ti substrate and cut into small pieces (1 cm × 1 cm). The resulting N-NTO NTAs and A-NTO NTAs pieces with exposed Ti substrate on the other side were used directly as the working electrode. Before assembling the coin cells, the working electrode was dried in a vacuum oven at 120 °C for 6 h. Pure Na foil was used as the counter electrode, and borosilicate glass microfiber (GF/D, Whatman) was employed as the separator. The electrolyte consisted of 1.0 M $NaClO_4$ in a mixed solution of ethylene carbonate and diethyl carbonate (1:1 by volume). All the assembled coin cells were rested overnight prior to electrochemical tests. Galvanostatic discharge/charge tests were performed on a Land CT2001A battery tester (China) in the voltage range of 0.01–2.5 V vs. Na^+/Na. A CHI 760D electrochemical workstation (USA) was adopted to carry out cyclic voltammogram and electrochemical impedance spectroscopy (EIS) analyses. The EIS was recorded in a frequency range from 100 kHz to 10 mHz with an amplitude of 5 mV. All the tests were conducted at room temperature.

2. Supplementary Figures

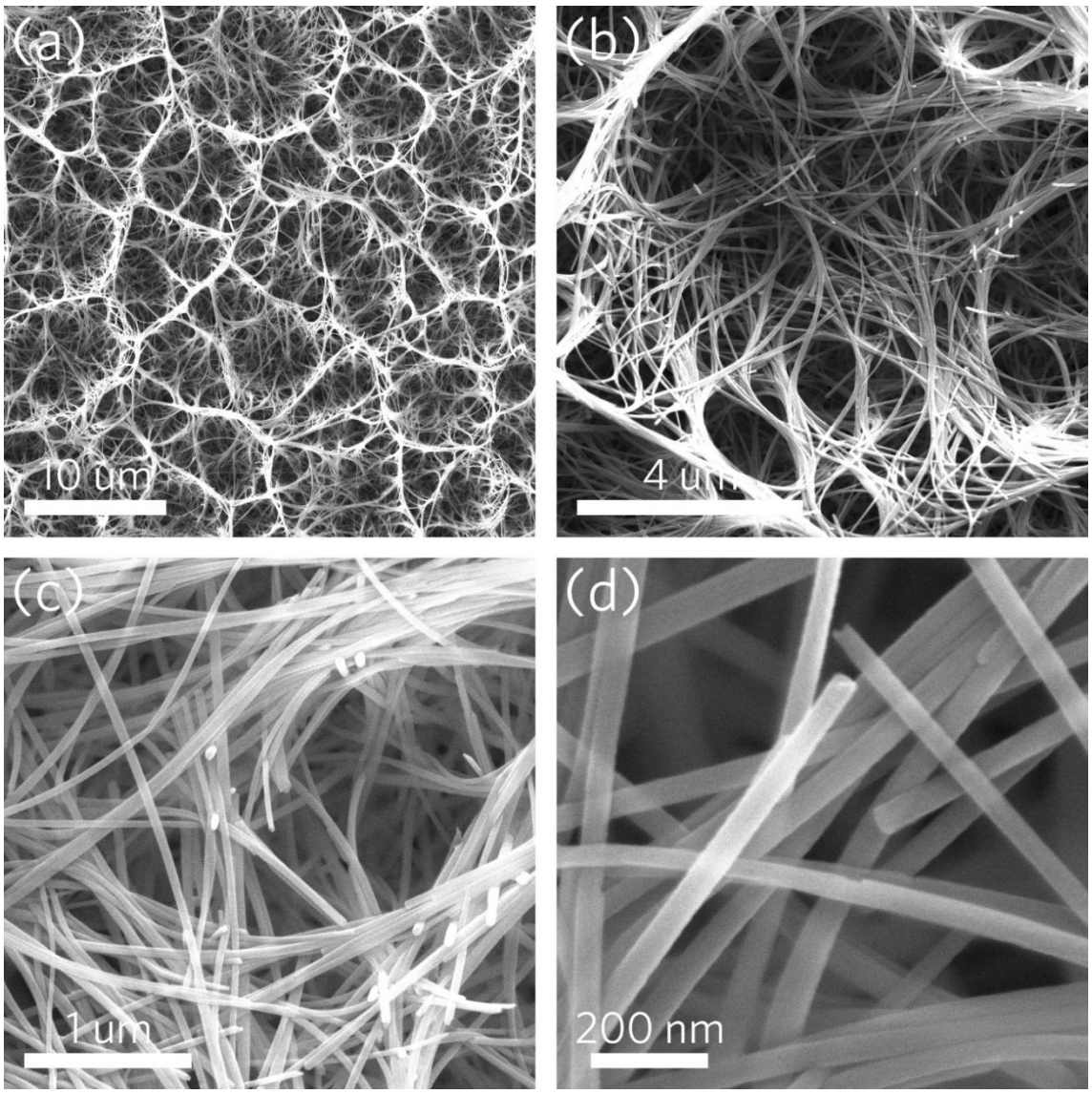

Figure S1. (a−d) SEM images of NTO NTAs under different magnifications.

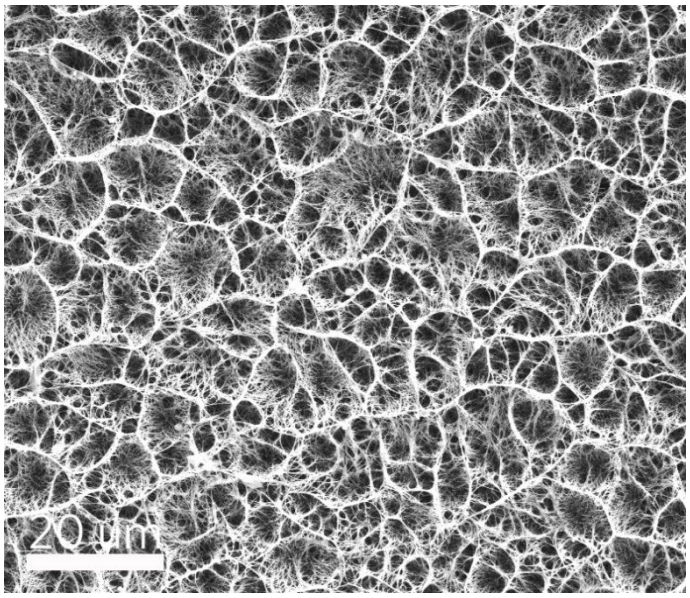

Figure S2. Low-magnification SEM image of N-NTO NTAs.

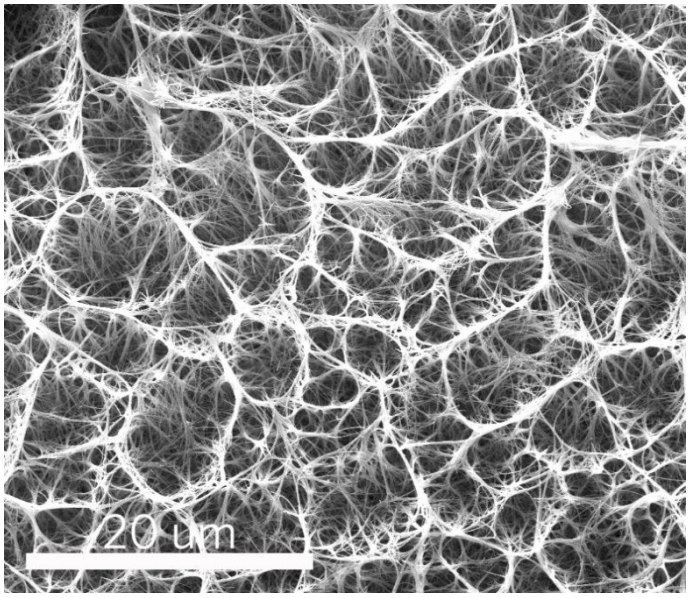

Figure S3. Low-magnification SEM image of A-NTO NTAs.

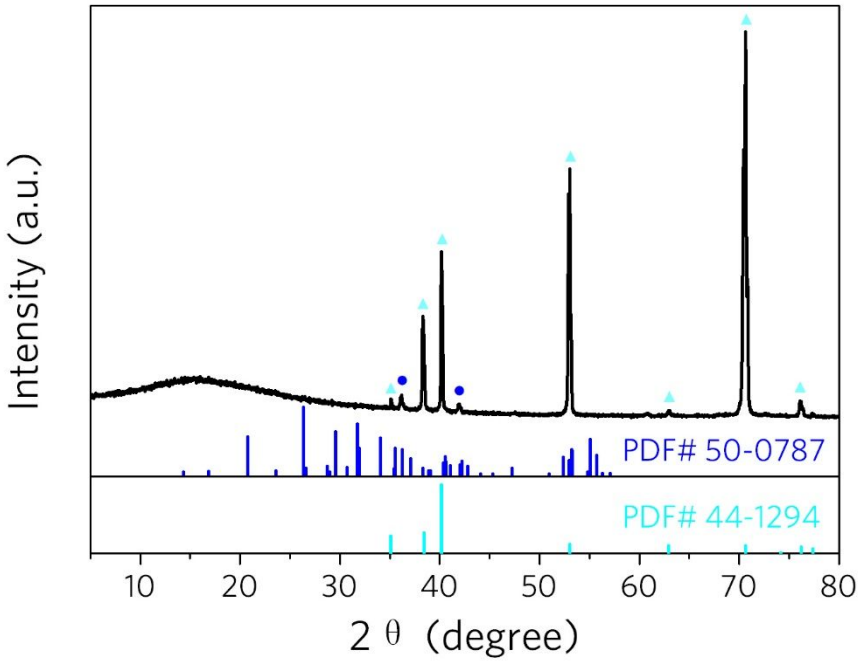

Figure S4. XRD pattern of Ti foil along with standard XRD pattern of Ti and Ti_4O_7 for reference. The Ti_4O_7 species should be attributed to the titanium surface oxidation in the air.

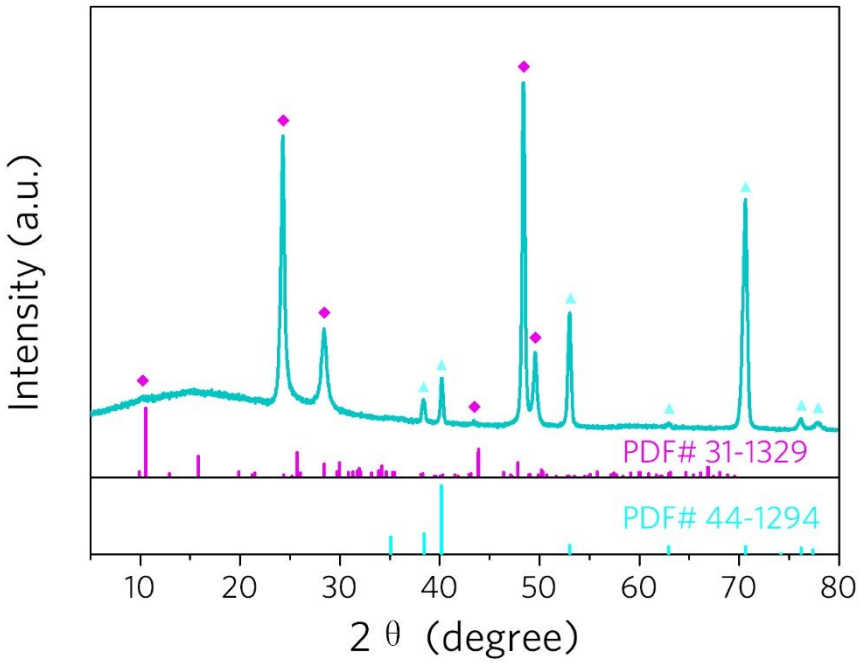

Figure S5. XRD pattern of NTO NTAs along with standard XRD pattern of $Na_2Ti_3O_7$ and Ti for reference.

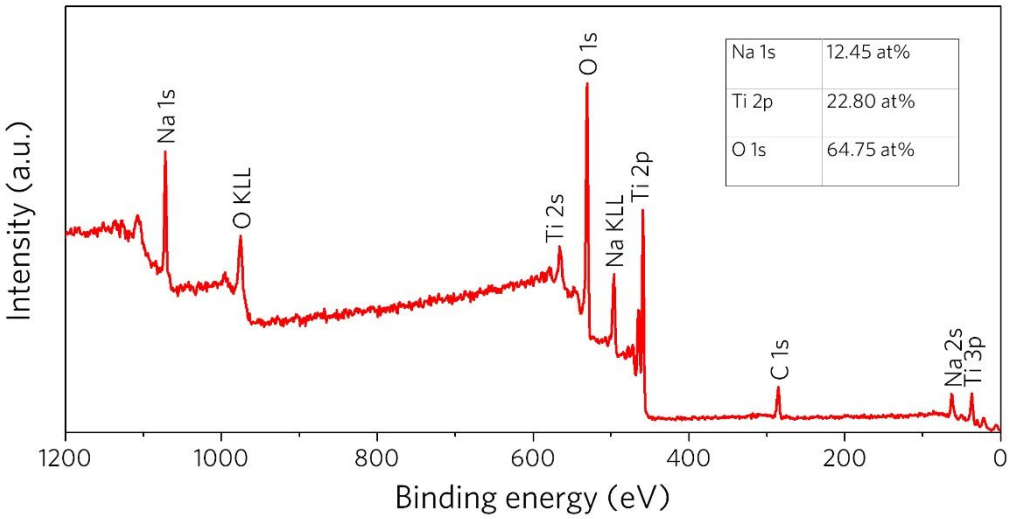

Figure S6. Survey XPS spectrum of N-NTO NTAs.

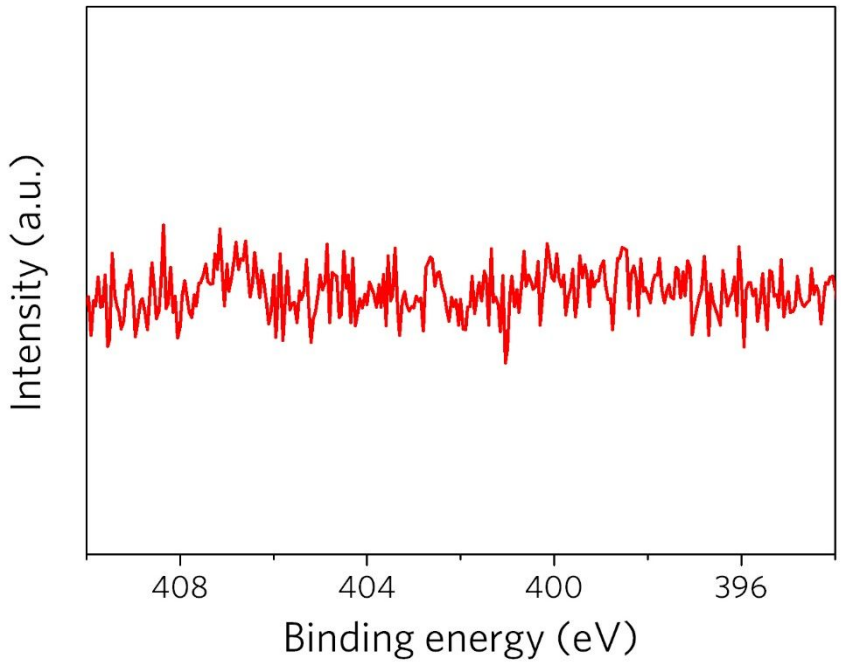

Figure S7. High-resolution XPS spectrum of N-NTO NTAs in the region of N 1s.

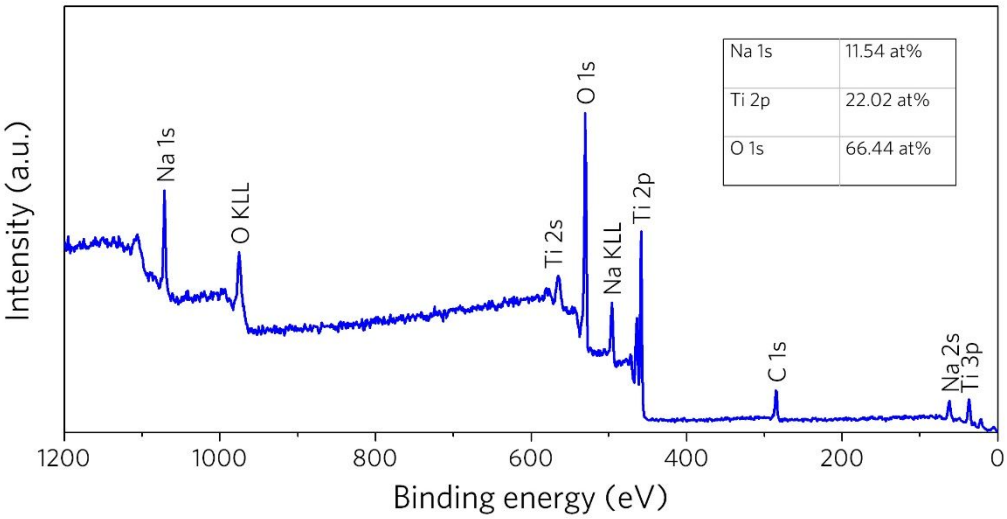

Figure S8. Survey XPS spectrum of A-NTO NTAs.

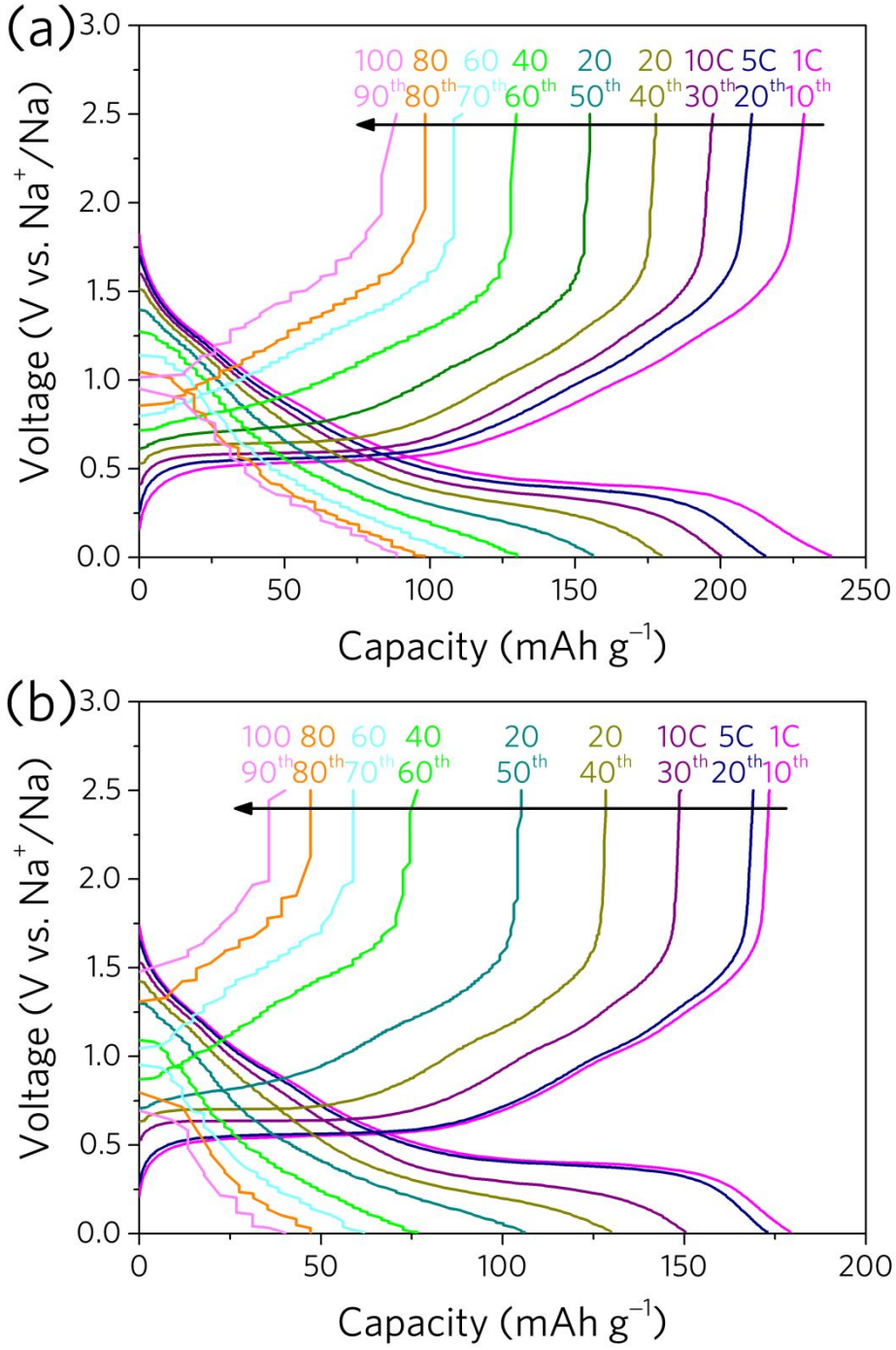

Figure S9. Galvanostatic discharge-charge profiles at different rates for (a) N-NTO NTAs and (b) A-NTO NTAs.

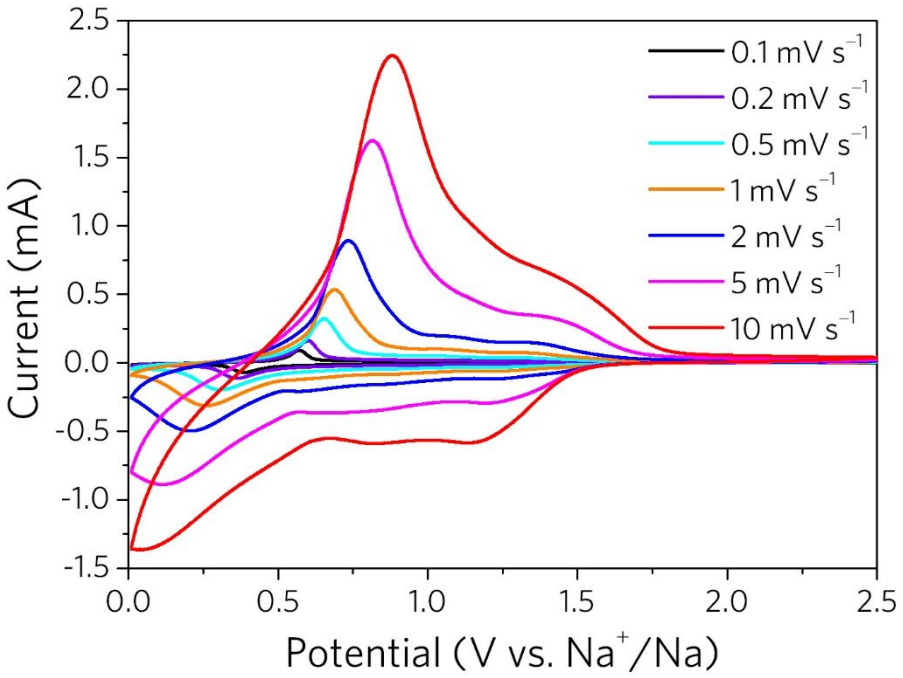

Figure S10. CV curves of N-NTO NTAs at different scan rates from 0.1 to 10 mV s^{-1}.

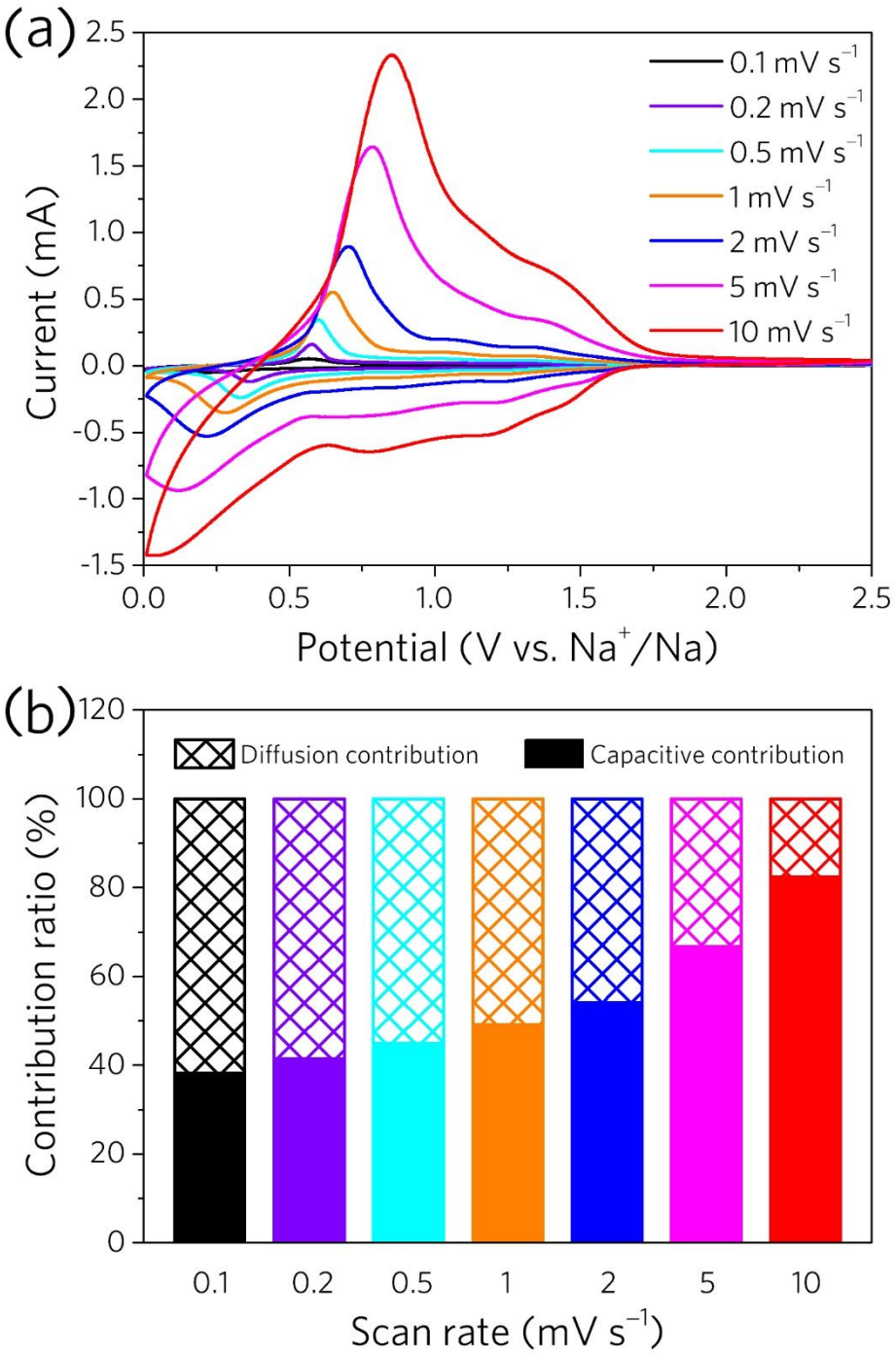

Figure S11. (a) CV curves of A-NTO NTAs at different scan rates from 0.1 to 10 mV s^{-1}, and (b) corresponding capacity contribution ratios to the total capacity.

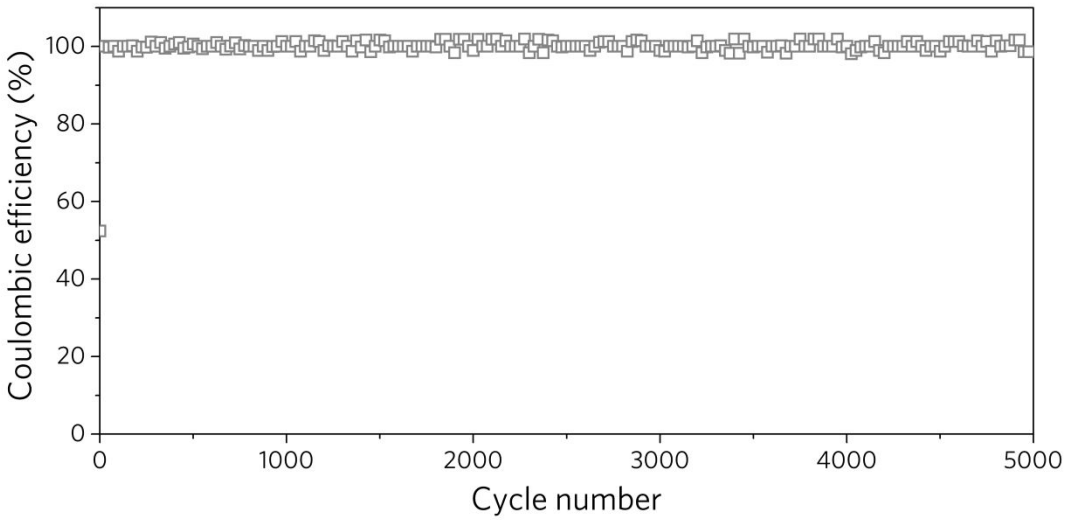

Figure S12. Coulombic efficiency of A-NTO NTAs during the prolonged cycling test.

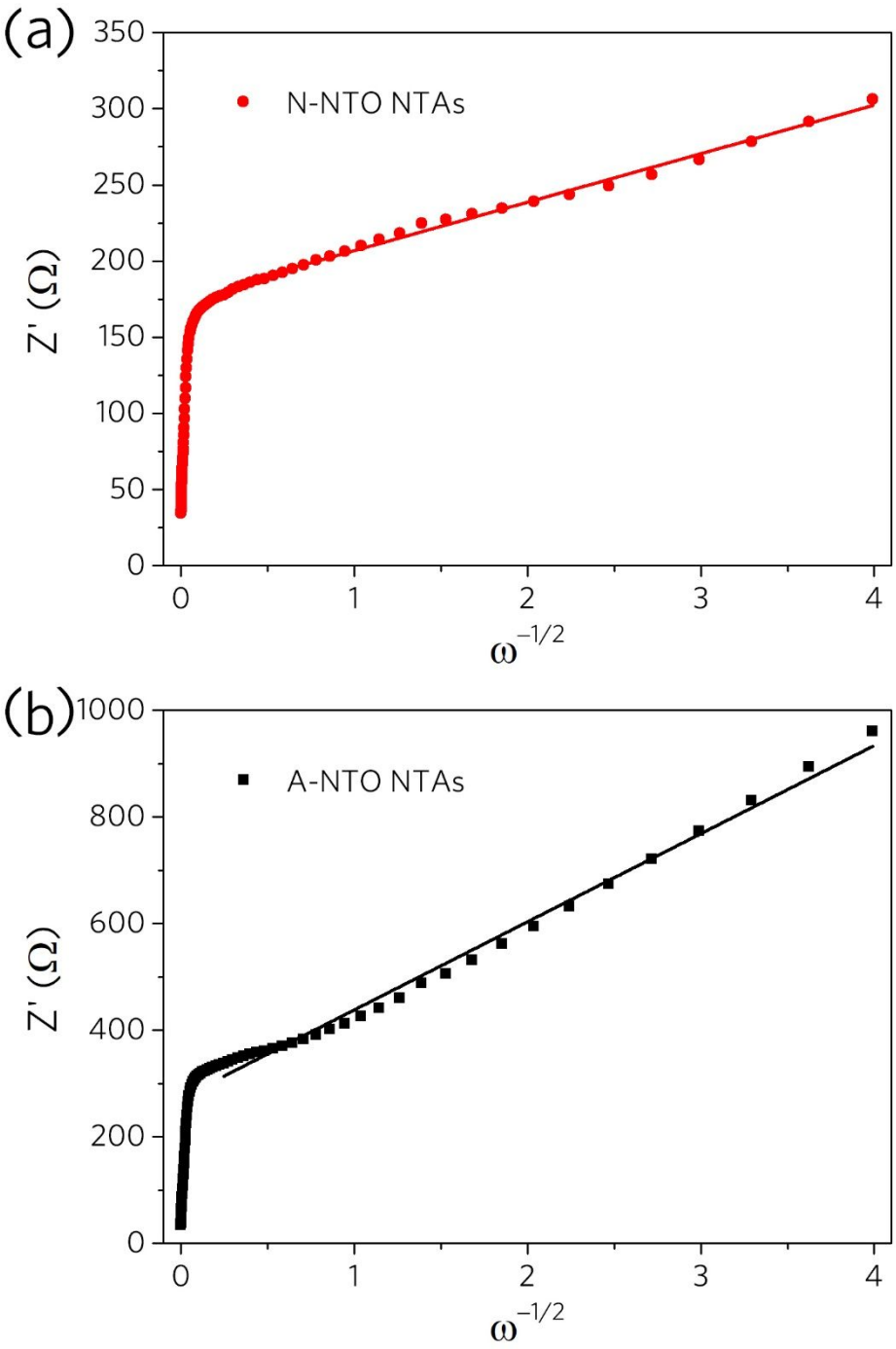

Figure S13. The linear fitting between the real part of impedance (Z') and the inverse square root of angular frequency ($\omega^{-1/2}$) in the low frequency region for (a) N-NTO NTAs and (b) A-NTO NTAs.

3. Supplementary Tables

Table S1. Summary and comparison of cycling and rate performances of recently reported $Na_2Ti_3O_7$ based anodes for SIBs

Materials	Voltage range (V vs. Na^+/Na)	Cycling performance			Rate performance		Reference
		Capacity (mAh g^{-1})	Cycles	Current (A g^{-1})	Capacity (mAh g^{-1})	Current (A g^{-1})	
N-NTO NTAs	0.01−2.5	117.8	5000	8.85	237.9, 215.3, 200.1, 179.6, 156, 129.8, 111.1, 98.2, and 88.5	0.177, 0.354, 0.885, 1.77, 3.54, 7.08, 10.62, 14.16, and 17.70	This work
$Na_2Ti_3O_7$@C HHSs	0.01−2.5	68	1000	8.8	210, 179, 142, 120, 94, 82, and 63	0.177, 0.354, 0.885, 1.77, 3.54, 5.31, and 8.85	1
$Na_2Ti_3O_7$@RHCS	0.01−2.5	70.62	1000	3.54	175.52, 148.57, 114.65, 86.26, 66.65, 55.73, and 45.71	0.177, 0.354, 0.885, 1.77, 3.54, 5.31, and 8.85	2
$Na_2Ti_3O_7$@C FNFs	0.01−2.5	58	1500	8.85	164, 135, 127, 110, 96, 87, 78, 71, and 63	0.0885, 0.177, 0.354, 0.885, 1.77, 3.54, 5.31, 7.08, and 8.85	3
$Na_2Ti_3O_7$/C	0.01−2.5	~40	1500	0.178	86, 80, 78, 75, 71, 68, 64, and 55	0.0356, 0.178, 0.356, 0.89, 1.78, 3.56, 7.12, and 14.24	4
$Na_2Ti_3O_7$/C	0.01−2.5	72.8	100	0.89	133.4, 121.2, 104.3, and 79.5	0.089, 0.178, 0.356, and 0.89	5
$Na_2Ti_3O_7$@C NTs	0.01−2.5	142.2	100	0.311	220, 180, 170, 150, 137, 108, and 84	0.0311, 0.0622, 0.1555, 0.311, 0.622, 1.555, and 3.11	6
NTO-rGO	0.05−2.5	135	650	0.5	226, 186, 166, 152, and 135	0.05, 0.1, 0.2, 0.3, and 0.5	7
$Na_2Ti_3O_7$/rGO	0.01−2.5	133.8	300	0.1	325, 250, 200, 175, 152, 132, and 116	0.02, 0.04, 0.1, 0.2, 0.4, 1.0, and 2.0	8
S-NTO NW@CNT+rGO	0.01−2.5	80.6	150	0.885	204.8, 162, 115.5, 86.5, 56, and 31.9	0.0354, 0.0885, 0.177, 0.354, 0.885, and 1.77	9
NTO/CF	0.01−2.5	98.8	2000	2.0	~186, ~170, ~147, ~119, ~87, and ~57	0.2, 0.5, 1.0, 2.0, 3.0, and 4.0	10
NTO nanowires@CC	0.01−2.5	100.6	500	0.531	297.8, 242,8, 191.5, 169.9, 119.2, and 54.9	0.0885, 0.177, 0.354, 0.531, 0.708, and 0.885	11
Twine-like $Na_2Ti_3O_7$ nanotubes	0.01−2.5	85	1000	1.77	157, 154, 148, 139, 130, 123, 110, 102, and 80	0.0354, 0.0885, 0.177, 0.354, 0.885, 1.77, 3.54, 5.31, and 8.85	12

Yb-doped NTO	0.01−2.5	71.6	1500	0.89	153.1, and 89.4	0.178, and 5.34	13
NTO-2.5	0.05−2.5	95	100	0.178	192, and 101	0.0178, and 0.712	14
Spider web-like $Na_2Ti_3O_7$ nanotubes	0.005−2.5	107	500	0.5	250, 200, 150, 125, and 100	0.1, 0.2, 0.5, 1.0, and 3.0	15
Hydrogenated $Na_2Ti_3O_7$ nanoarrays	0.1−2.5	65	10000	6.2	227, 210, 190, 164, 130, 99, 77, and 71	0.0354, 0.0885, 0.177, 0.354, 0.885, 1.77, 3.54, and 6.2	16
95% $Na_2Ti_3O_7$/5 % $Na_2Ti_6O_{13}$	0.01−2.5	68	100	0.89	170, 115, and 92	0.0356, 0.356, and 0.89	17
$Na_2Ti_3O_7$ nanotubes	0.01−2.5	176	100	0.6	220, and 155	0.1, and 2.0	18
ST-NTO	0.1−2.5	78	10000	1.77	287, 227, 186, 151, 111, and 84	0.0354, 0.0885, 0.177, 0.354, 0.885, and 1.77	19
3D $Na_2Ti_3O_7$ microflowers	0.01−2.5	~85	1100	0.4	173.4, 121.3, 99.7, 84.6, and 73.8	0.05, 0.1, 0.2, 0.4, and 0.8	20
$Na_2Ti_3O_7$ nanofibers	0−2.5	98.6	100	0.03	206.9, 161.8, 116.5, and 72.4	0.05, 0.1, 0.2, and 0.4	21
$Na_2Ti_3O_7$ NP-NS	0.1−2.5	110	300	0.5	160, and 110	0.1, and 1.0	22

Table S2. Summary and comparison of cycling and rate performances of recently reported transition metal related anodes for SIBs

Materials	Voltage range (V vs. Na^+/Na)	Cycling performance			Rate performance		Reference
		Capacity (mA h g^{-1})	Cycles	Current (A g^{-1})	Capacity (mA h g^{-1})	Current (A g^{-1})	
N-NTO NTAs	0.01−2.5	117.8	5000	8.85	237.9, 215.3, 200.1, 179.6, 156, 129.8, 111.1, 98.2, and 88.5	0.177, 0.354, 0.885, 1.77, 3.54, 7.08, 10.62, 14.16, and 17.70	This work
P-TiO_2 array	0.1−2.5	141	1000	3.35	334, 256, and 147	0.067, 0.335, and 3.35	23
TiO_2 SNTs	0.05−3.0	107	4000	5.68	191, 170, 148, 129, 110, and 94	0.355, 0.71, 1.42, 2.84, 5.68, and 11.36	24
TiO_2∩NPCSs	0.01−3.0	114	10000	3.35	201, 171, 157, 149, 133, 119, 100, 87, 85, and 80	0.084, 0.168, 0.335, 0.67, 1.675, 3.35, 6.7, 10.05, 13.4, and 16.75	25
TiO_{2-x}/N-doped carbon fibers	0.05−3.0	210	100	0.1	230, 200, 176, 145, and 120	0.05, 0.1, 0.2, 0.5, and 1.0	26
TiO_2(A/B)-MS	0.01−2.0	~130	1000	2.5	~214, ~205, ~191, ~178, ~154, ~142, ~120, ~93, ~71, and ~45	0.025, 0.05, 0.125, 0.25, 0.75, 1.25, 2.5, 5.0, 7.5, and 12.5	27
Mesocrystal TiO_2 hollow sphere	0.01−3.0	110	1000	1.0	255, 215, 194, 170, 156, 148, and 142	0.05, 0.1, 0.2, 0.5, 1.0, 1.5, and 2.0	28
2D mesoporous TiO_2 NS	0.01−3.0	44	10000	10	183, 156, 119, 88, and 67	0.2, 0.5, 1.0, 2.0, 5.0, and 10.0	29
MXene-derived $NaTi_{1.5}O_{8.3}$	0.01−3.0	116	150	0.2	196, 169, 153, 134, 119, 109, and 101	0.05, 0.1, 0.2, 0.5, 1.0, 1.5, and 2.0	30
$NaV_{1.25}Ti_{0.75}O_4$	0.2−2.3	~87	1000	0.1	103, 92, 81, 68, 52, and 40	0.02, 0.05, 0.1, 0.2, 0.5, and 1.0	31
C-coated $Ni_{0.5}TiOPO_4$	0.2−3.0	~172	100	0.28	280, 250, 210, 190, and 130	0.028, 0.07, 0.14, 0.28, and 0.7	32
Co_3O_4@C	0.001−3.0	228	150	0.5	583, 416, 310, 251, and 183	0.1, 0.2, 0.5, 1.0, and 2.0	33
M-V_2O_3	0.1−2.2	90	5300	2.0	357, 284, 242, 200, 167, and 136	0.05, 0.1, 0.2, 0.5, 1.0, and 2.0	34
CaV_4O_9-550	0.01−3.0	149.8	1600	1.0	265.2, 250.5, 225.3, 183.2, 146.1, and 103.4	0.1, 0.3, 0.5, 1.0, 2.0, and 5.0	35
Fe_2GeO_4@C	0.01−3.0	376.5	100	0.1	~422, ~394, ~357, ~316, and ~211	0.1, 0.2, 0.5, 1.0, and 2.0	36

Rodlike $CoMoO_4$	0.005−2.7	229	100	0.049	360, 317, 274, 221, and 165	0.049, 0.098, 0.245, 0.49, and 0.98	37
N-doped C@$Zn_3B_2O_6$	0−3.0	257.3	30	0.1	357.8, 282.4, 217.4, and 172.8	0.1, 0.2, 0.5, and 1.0	38
$Ti_2Nb_2O_9$ nanosheets	0.01−3.0	~170	500	0.8	242, 229, 208, 182, 157, and 134	0.1, 0.2, 0.5, 1.0, 2.0, and 4.0	39
CoP_3@C	0−2.5	145.5	260	0.3	344.1, 244.5, 194.4, 169.6, 153.8, and 136.4	0.025, 0.05, 0.1, 0.15, 0.2, and 0.25	40
M13-ZnS600C	0−3.0	178	100	0.1	~428, ~297, ~216, ~166, and ~59	0.05, 0.1, 0.2, 0.3, and 0.4	41
WP/CC	0.01−3.0	50	1000	2.0	502, 331, 194, 111, and 56	0.1, 0.2, 0.5, 1.0, and 2.0	42
AC@SnS-SnS_2	0.005−3.0	230	500	0.1	380, and 110	0.05, and 5.0	43
Nanoparticle Cu_2GeS_3	0.005−2.0	253.9	100	0.1	304, 252, 185, and 152	0.05, 0.1, 0.2, and 0.5	44

4. Supplementary References

(1) Xie, F.; Zhang, L.; Su, D.; Jaroniec, M.; Qiao, S. Z. $Na_2Ti_3O_7$@N-Doped Carbon Hollow Spheres for Sodium-Ion Batteries with Excellent Rate Performance. *Adv. Mater.* **2017**, *29*, 1700989.

(2) Chen, S.; Pang, Y.; Liang, J.; Ding, S. Red Blood Cell-Like Hollow Carbon Sphere Anchored Ultrathin $Na_2Ti_3O_7$ Nanosheets as Long Cycling and High Rate-Performance Anodes for Sodium-Ion Batteries. *J. Mater. Chem. A* **2018**, *6*, 13164−13170.

(3) Nie, S.; Liu, L.; Li, M.; Liu, J.; Xia, J.; Zhang, Y.; Wang, X. $Na_2Ti_3O_7$/C Nanofibers for High-Rate and Ultralong-Life Anodes in Sodium-Ion Batteries. *ChemElectroChem* **2018**, *5*, 3498−3505.

(4) Rudola, A.; Sharma, N.; Balaya, P. Introducing a 0.2V Sodium-Ion Battery Anode: The $Na_2Ti_3O_7$ to $Na_{3-x}Ti_3O_7$ Pathway. *Electrochem. Commun.* **2015**, *61*, 10−13.

(5) Yan, Z.; Liu, L.; Shu, H.; Yang, X.; Wang, H.; Tan, J.; Zhou, Q.; Huang, Z.; Wang, X. A Tightly Integrated Sodium Titanate-Carbon Composite as an Anode Material for Rechargeable Sodium Ion Batteries. *J. Power Sources* **2015**, *274*, 8−14.

(6) Li, M.; Xiao, X.; Fan, X.; Huang, X.; Liu, Y.; Chen, L. Carbon Coated Sodium-Titanate Nanotube as an Advanced Intercalation Anode Material for Sodium-Ion Batteries. *J. Alloys Compd.* **2017**, *712*, 365−372.

(7) Bi, R.; Zeng, C.; Ma, T.; Etogo, A.; Wang, X.; Zhang, L. Encapsulated Hollow $Na_2Ti_3O_7$ Spheres in Reduced Graphene Oxide Films for Flexible Sodium-Ion Batteries. *Electrochim. Acta* **2018**, *284*, 287−293.

(8) Zhou, Z.; Xiao, H.; Zhang, F.; Zhang, X.; Tang, Y. Solvothermal Synthesis of $Na_2Ti_3O_7$ Nanowires Embedded in 3D Graphene Networks as an Anode for High-Performance Sodium-Ion Batteries. *Electrochim. Acta* **2016**, *211*, 430−436.

(9) Li, Z.; Ye, S.; Wang, W.; Xu, Q.; Liu, H.; Wang, Y.; Xia, Y. Free-Standing Sandwich-Structured Flexible Film Electrode Composed of $Na_2Ti_3O_7$ Nanowires@CNT and Reduced Graphene Oxide for Advanced Sodium-Ion Batteries. *ACS Omega* **2017**, *2*, 5726−5736.

(10) Dong, S.; Wu, L.; Wang, J.; Nie, P.; Dou, H.; Zhang, X. Self-Supported Electrodes of $Na_2Ti_3O_7$ Nanoribbon Array/Graphene Foam and Graphene Foam for Quasi-Solid-State Na-Ion Capacitors. *J. Mater. Chem. A* **2017**, *5*, 5806−5812.

(11) Li, Z.; Shen, W.; Wang, C.; Xu, Q.; Liu, H.; Wang, Y.; Xia, Y. Ultra-Long $Na_2Ti_3O_7$ Nanowires@Carbon Cloth as a Binder-Free Flexible Electrode with a Large Capacity and Long Lifetime for Sodium-Ion Batteries. *J. Mater. Chem. A* **2016**, *4*, 17111−17120.

(12) Yan, X.; Sun, D.; Jiang, J.; Yan, W.; Jin, Y. Self-Assembled Twine-Like $Na_2Ti_3O_7$ Nanostructure as Advanced Anode for Sodium-Ion Batteries. *J. Alloys Compd.* **2017**, *697*, 208−214.

(13) Xia, J.; Zhao, H.; Pang, W. K.; Yin, Z.; Zhou, B.; He, G.; Guo, Z.; Du, Y. Lanthanide Doping Induced Electrochemical Enhancement of $Na_2Ti_3O_7$ Anodes for Sodium-Ion Batteries. *Chem. Sci.* **2018**, *9*, 3421−3425.

(14) Zou, W.; Fan, C.; Li, J. Sodium Titanate/Carbon ($Na_2Ti_3O_7$/C) Nanofibers via Electrospinning Technique as the Anode of Sodium-Ion Batteries. *Chin. J. Chem.* **2017**, *35*, 79−85.

(15) Zhang, Y.; Guo, L.; Yang, S. Three-Dimensional Spider-Web Architecture Assembled from $Na_2Ti_3O_7$ Nanotubes as a High Performance Anode for a Sodium-Ion Battery. *Chem. Commun.* **2014**, *50*, 14029−14032.

(16) Fu, S.; Ni, J.; Xu, Y.; Zhang, Q.; Li, L. Hydrogenation Driven Conductive $Na_2Ti_3O_7$ Nanoarrays as Robust Binder-Free Anodes for Sodium-Ion Batteries. *Nano Lett.* **2016**, *16*, 4544−4551.

(17) Ho, C. K.; Li, C. Y. V.; Chan, K. Y. Scalable Template-Free Synthesis of $Na_2Ti_3O_7$/$Na_2Ti_6O_{13}$ Nanorods with Composition Tunable for Synergistic Performance in Sodium-Ion Batteries. *Ind. Eng. Chem. Res.* **2016**, *55*, 10065−10072.

(18) Liu, Y.; Fang, X.; Zhang, A.; Shen, C.; Liu, Q.; Enaya, H. A.; Zhou, C. Layered P2-$Na_{2/3}[Ni_{1/3}Mn_{2/3}]O_2$ as High-Voltage Cathode for Sodium-Ion Batteries: The Capacity Decay Mechanism and Al_2O_3 Surface Modification. *Nano Energy* **2016**, *27*, 27−34.

(19) Ni, J.; Fu, S.; Wu, C.; Zhao, Y.; Maier, J.; Yu, Y.; Li, L. Superior Sodium Storage in $Na_2Ti_3O_7$ Nanotube Arrays through Surface Engineering. *Adv. Energy Mater.* **2016**, *6*, 1502568.

(20) Anwer, S.; Huang, Y.; liu, J.; Liu, J.; Xu, M.; Wang, Z.; Chen, R.; Zhang, J.; Wu, F. Nature-Inspired $Na_2Ti_3O_7$ Nanosheets-Formed Three-Dimensional Microflowers Architecture as a High-Performance Anode Material for Rechargeable Sodium-Ion Batteries. *ACS Appl. Mater. Interfaces* **2017**, *9*, 11669−11677.

(21) Ge, Y.; Zhu, J.; Dirican, M.; Jia, H.; Yanilmaz, M.; Lu, Y.; Chen, C.; Qiu, Y.; Zhang, X. Fabrication and Electrochemical Behavior Study of Nano-Fibrous Sodium Titanate Composite. *Mater. Lett.* **2017**, *188*, 176−179.

(22) Ko, J. S.; Doan-Nguyen, V. V. T.; Kim, H. S.; Muller, G. A.; Serino, A. C.; Weiss, P. S.; Dunn, B. S. $Na_2Ti_3O_7$ Nanoplatelets and Nanosheets Derived from a Modified Exfoliation Process for Use as a High-Capacity Sodium-Ion Negative Electrode. *ACS Appl. Mater. Interfaces* **2017**, *9*, 1416−1425.

(23) Ni, J.; Fu, S.; Yuan, Y.; Ma, L.; Jiang, Y.; Li, L.; Lu, J. Boosting Sodium Storage in TiO_2 Nanotube Arrays through Surface Phosphorylation. *Adv. Mater.* **2018**, *30*, 1704337.

(24) Chen, B.; Meng, Y.; Xie, F.; He, F.; He, C.; Davey, K.; Zhao, N.; Qiao, S.-Z. 1D Sub-Nanotubes with Anatase/Bronze TiO_2 Nanocrystal Wall for High-Rate and Long-Life Sodium-Ion Batteries. *Adv. Mater.* **2018**, *30*, 1804116.

(25) Li, B.; Xi, B.; Wu, F.; Mao, H.; Liu, J.; Feng, J.; Xiong, S. One-Step In Situ Formation of N-doped Carbon Nanosheet 3D Porous Networks/TiO_2 Hybrids with Ultrafast Sodium Storage. *Adv. Energy Mater.* **2019**, *9*, 1803070.

(26) Zhao, Q.; Bi, R.; Cui, J.; Yang, X.; Zhang, L. TiO_{2-x} Nanocages Anchored in N-Doped Carbon Fiber Films as a Flexible Anode for High-Energy Sodium-Ion Batteries. *ACS Appl. Energy Mater.* **2018**, *1*, 4459−4466.

(27) Hwang, J.-Y.; Du, H.-L.; Yun, B.-N.; Jeong, M.-G.; Kim, J.-S.; Kim, H.; Jung, H.-G.; Sun, Y.-K. Carbon-Free TiO_2 Microspheres as Anode Materials for Sodium Ion Batteries. *ACS Energy Lett.* **2019**, *4*, 494−501.

(28) Yang, R.; Sun, L.; Liu, W.; Zhang, Y.; Cui, Y.; Du, Y.; Liu, S.; Wang, H.; Huang, M. Bio-derived 3D TiO_2 Hollow Spheres with a Mesocrystal Nanostructure to Achieve Improved Electrochemical Performance of Na-Ion Batteries in Ether-Based Electrolytes. *J. Mater. Chem. A* **2019**, *7*, 3399−3407.

(29) Lan, K.; Liu, Y.; Zhang, W.; Liu, Y.; Elzatahry, A.; Wang, R.; Xia, Y.; Al-Dhayan, D.; Zheng, N.; Zhao, D. Uniform Ordered Two-Dimensional Mesoporous TiO_2 Nanosheets from Hydrothermal-Induced Solvent-Confined Monomicelle Assembly. *J. Am. Chem. Soc.* **2018**, *140*, 4135−4143.

(30) Dong, Y.; Wu, Z. S.; Zheng, S.; Wang, X.; Qin, J.; Wang, S.; Shi, X.; Bao, X. Ti_3C_2 MXene-Derived Sodium/Potassium Titanate Nanoribbons for High-Performance Sodium/Potassium Ion Batteries with Enhanced Capacities. *ACS Nano* **2017**, *11*, 4792−4800.

(31) Liu, J.; Zheng, Y.; Wang, Z.; Lu, Z.; Vasileff, A.; Qiao, S.-Z. Free-Standing Single-Crystalline NiFe-Hydroxide Nanoflake Arrays: A Self-Activated and Robust Electrocatalyst For Oxygen Evolution. *Chem. Commun.* **2018**, *54*, 463−466.

(32) Nassiri, A.; Sabi, N.; Sarapulova, A.; Dahbi, M.; Indris, S.; Ehrenberg, H.; Saadoune, I. $Ni_{0.5}TiOPO_4$ Phosphate: Sodium Insertion Mechanism and Electrochemical Performance in Sodium-Ion Batteries. *J. Power Sources* **2019**, *418*, 211−217.

(33) Zhou, Y.; Sun, W.; Rui, X.; Zhou, Y.; Ng, W. J.; Yan, Q.; Fong, E. Biochemistry-Derived Porous Carbon-Encapsulated Metal Oxide Nanocrystals for Enhanced Sodium Storage. *Nano Energy* **2016**, *21*, 71−79.

(34) Sarkar, A.; Sinha, A. K.; Mitra, S. Nanostructured Vanadium Tri-Oxides, as a Long Life and High Performance Anode for Sodium-Ion Battery. *Electrochim. Acta* **2019**, *299*, 914−925.

(35) Xu, X.; Niu, C.; Duan, M.; Wang, X.; Huang, L.; Wang, J.; Pu, L.; Ren, W.; Shi, C.; Meng, J.; Song, B.; Mai, L. Alkaline Earth Metal Vanadates as Sodium-Ion Battery Anodes. *Nat. Commun.* **2017**, *8*, 460.

(36) Subramanian, Y.; Park, M. S.; Veerasubramani, G. K.; Lee, Y.-S.; Kim, D.-W. Synthesis and Electrochemical Performance of Carbon-Coated Fe_2GeO_4 as an Anode Material for Sodium-Ion Batteries. *Mater. Chem. Phys.* **2019**, *224*, 129−136.

(37) Ali, G.; Islam, M.; Kim, J. Y.; Jung, H.-G.; Chung, K. Y. Kinetic and Electrochemical Reaction Mechanism Investigations of Rodlike $CoMoO_4$ Anode Material for Sodium-Ion Batteries. *ACS Appl. Mater. Interfaces* **2019**, *11*, 3843−3851.

(38) Wang, S.; Zhang, X. B. N-Doped C@$Zn_3B_2O_6$ as a Low Cost and Environmentally Friendly Anode Material for Na-Ion Batteries: High Performance and New Reaction Mechanism. *Adv. Mater.* **2019**, *31*, 1805432.

(39) Shen, L.; Wang, Y.; Lv, H.; Chen, S.; van Aken, P. A.; Wu, X.; Maier, J.; Yu, Y. Ultrathin $Ti_2Nb_2O_9$ Nanosheets with Pseudocapacitive Properties as Superior Anode for Sodium-Ion Batteries. *Adv. Mater.* **2018**, *30*, 1804378.

(40) Zhao, W.; Ma, X.; Wang, G.; Long, X.; Li, Y.; Zhang, W.; Zhang, P. Carbon-Coated CoP_3 Nanocomposites as Anode Materials for High-Performance Sodium-Ion Batteries. *Appl. Surf. Sci.* **2018**, *445*, 167−174.

(41) Zhang, G.; Wei, S.; Belcher, A. M. Biotemplated Zinc Sulfide Nanofibers as Anode Materials for Sodium-Ion Batteries. *ACS Appl. Nano Mater.* **2018**, *1*, 5631−5639.

(42) Pan, Q.; Chen, H.; Wu, Z.; Wang, Y.; Zhong, B.; Xia, L.; Wang, H.-Y.; Cui, G.; Guo, X.; Sun, X. Nanowire of WP as a High-Performance Anode Material for Sodium-Ion Batteries. *Chem. Eur. J.* **2019**, *25*, 971−975.

(43) Zhang, S. W.; Lv, W.; Qiu, D.; Cao, T.; Zhang, J.; Lin, Q.; Chen, X.; He, Y.-B.; Kang, F.; Yang, Q.-H. An Ion-Conducting SnS–SnS_2 Hybrid Coating for Commercial Activated Carbons Enabling their Use as High Performance Anodes for Sodium-Ion Batteries. *J. Mater. Chem. A* **2019**, *7*, 10761−10768.

(44) Fu, L.; Shang, C.; Ma, J.; Zhang, C.; Zang, X.; Chai, J.; Li, J.; Cui, G. Cu_2GeS_3 Derived Ultrafine Nanoparticles as High-Performance Anode for Sodium Ion Battery. *Sci. China Mater.* **2018**, *61*, 1177−1184.